Hindawi
International Journal of Antennas and Propagation
Volume 2018, Article ID 5634826, 9 pages
https://doi.org/10.1155/2018/5634826

Research Article

Indoor Propagation of Electromagnetic Waves with Orbital Angular Momentum at 5.8 GHz

Boseok Jeong, Hayeon Kim, and Haengseon Lee

Department of Electronic Engineering, Sogang University, 1 Sinsu-dong, Mapo-gu, Seoul, Republic of Korea

Correspondence should be addressed to Haengseon Lee; leehs95@sogang.ac.kr

Received 15 June 2017; Revised 17 November 2017; Accepted 18 December 2017; Published 31 January 2018

Academic Editor: Paolo Baccarelli

Propagation of electromagnetic waves with orbital angular momentum (OAM) is investigated in indoor environments. The OAM modes generated by circular patch array antennas are used. With proper alignment and suppressed multipath, the OAM modes can transport multiple wireless data stream at the same time. Through measurements and ray-tracing simulations, it is found that the advantages of OAM modes are limited if those two conditions are not satisfied. It is also found that multipath effect can be enervated by using narrow beam antennas.

1. Introduction

As the demand for high data rate wireless communication increases, various modulation schemes are devised in the frequency, time, and spatial domains like OFDM, TDMA, SDMA, and MIMO. Along with those approaches, orbital angular momentum (OAM) of electromagnetic waves receives interest in that it can increase the capacity of wireless communications. It is known that the electromagnetic radiation of antennas can be represented by a sum of eigenfunctions with distinct eigenvalues. For the case of spherical or cylindrical coordinate, the orbital angular momentums are associated with eigenvalue for the elevation or azimuth angles. Using the orthogonal properties of eigenfunctions, multiple data stream can be conveyed at the same time upon the eigenmodes without interfering one another, thus increasing the data rate.

The idea of OAM originated from the researches in optics field. It is known that Gaussian beams from laser beams can be decomposed into Laguerre-Gaussian modes using spiral phase plates [1]. The phase of each Laguerre-Gaussian mode changes by $2\pi L$ along the azimuth direction where L is an integer. The angular momentum of the mode is calculated as $L\hbar$, where $\hbar$ is the Planck constant and L is called the mode number [2]. Later, it was found that the same Laguerre-Gaussian modes can be generated at the microwave frequency using the same phase plate and a circular corrugated horn antenna [3]. Instead of spiral phase plates, arrays of antennas are used to generate OAM modes [4–7].

The orthogonality of OAM modes is utilized to increase the capacity of communication in the form of optical fiber [8] and wireless communication [9–11]. Recently, the influence of multipath fading is reported where received OAM modes are examined with antennas near metallic ground plane, where interferences between OAM modes with different eigenvalues are investigated [12].

In this paper, indoor propagations of OAM modes are investigated more extensively using experiments and ray-tracing simulations. Interferences between OAM modes after scattering are analyzed. The influences of antenna misalignment and beam width of antennas are also investigated. It is also shown that the capacity increase of OAM waves is limited by interference incurred by multipath fading, which is even aggravated with wide beam width antennas. By changing the beam width of element antennas, the condition for large indoor coverage is also derived.

2. Generation of OAM Modes

To investigate the indoor propagation of electromagnetic waves with OAM, circular array antennas are used as shown in Figure 1 [5]. The circular array antennas are convenient to

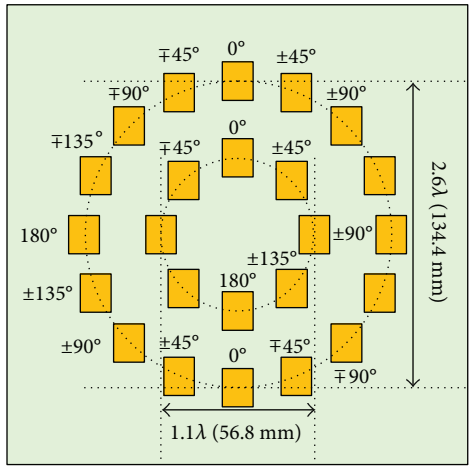

(a) Phases of element antennas

(b) Fabricated photo

Figure 1: Circular array antennas for generation of OAM modes $L = 1$ and 2.

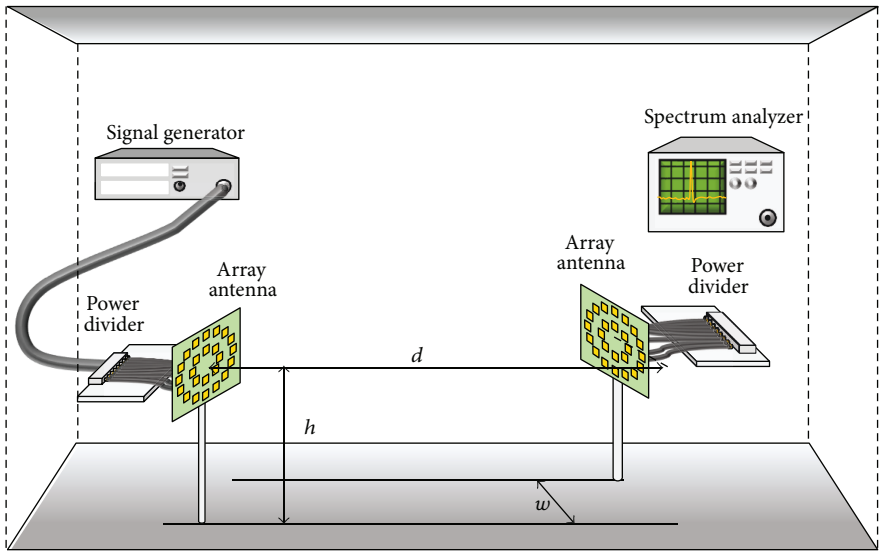

(a) Placement of antennas

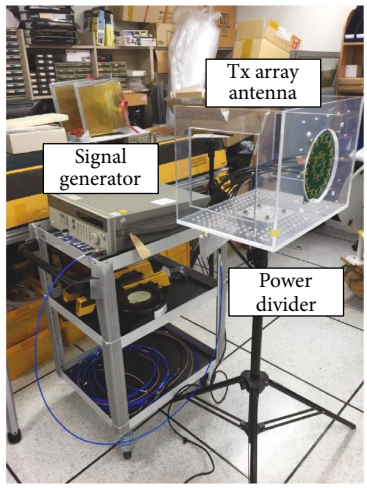

(b) Transmitter

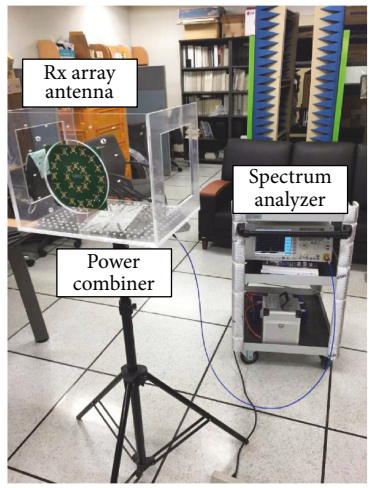

(c) Receiver

Figure 2: Experimental setup of the propagation of OAM waves.

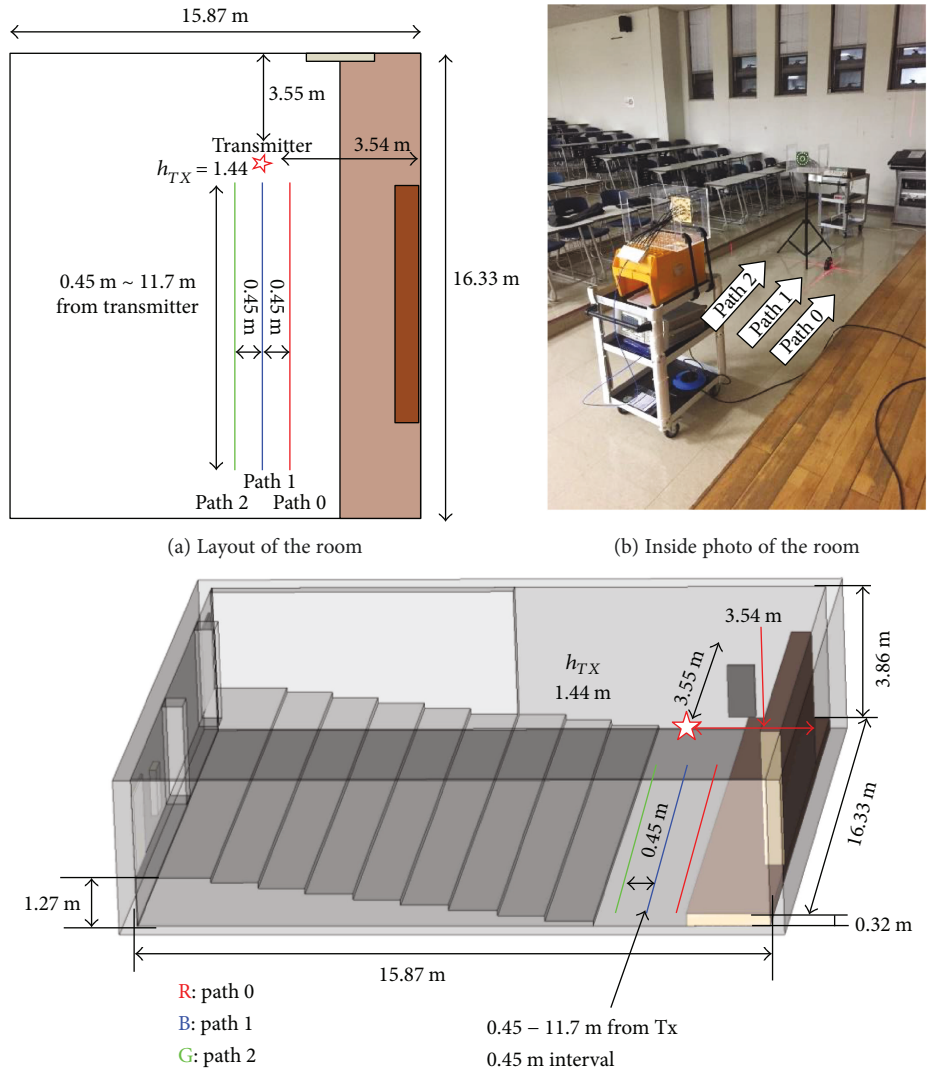

(a) Layout of the room

(b) Inside photo of the room

(c) Three-dimensional view of the room

Figure 3: Measurement site (lecture room).

generate OAM modes with different mode number L by changing the phase increment of adjacent elements [6, 7]. The design frequency is chosen to be 5.8 GHz that belongs to an unlicensed band. The element antenna has rectangular shape. For the generation of OAM mode of $L = 1$, eight elements are used. For other OAM modes such as $L = 2$, 16 elements can be used. The element antennas are arranged in circular shape, and their phases increase consecutively by 45°. The output of the signal generator is fed to the input ports of eight way power dividers whose outputs are then connected to coaxial cables whose lengths increase monotonically by 45°. Then, the cables are connected to input ports of element antennas. The patch arrays have advantage over phase plate approach, in that they have low profiles, but have disadvantage of complicated feed lines.

Figure 2 shows the experimental setup of OAM propagations. The transmitter is connected to a signal generator, and the receiver to a spectrum analyzer. The mode number of the transmitter is chosen from $L = 1$ or -1. That of the receiver is also chosen from $L = 1$ or -1. With the position of the transmitter fixed, received power levels are recorded as the receiver position is displaced. The measurements are done with the orientation of those antennas fixed. Alignment of those OAM antennas is changed by changing the transverse displacement w.

Figure 2 shows measurement setup of OAM wave propagations. The OAM modes of the transmitter and the receiver can be selected from $L = 1$ or -1. As the receiver moves along the paths farther away from the transmitter, received power levels are recorded by reading a spectrum analyzer. The influence of the antenna alignment is examined by choosing three paths with different ws. Measurements are performed in the lecture room and the corridor. The transmitter output power is 0 dBm, and the total cable loss is −7.5 dB.

3. Propagation in the Room

The first measurement site is a large lecture room whose layout is in Figure 3(a). The height of the ceiling is 3.86 m. The antennas for the transmitter and the receiver are at

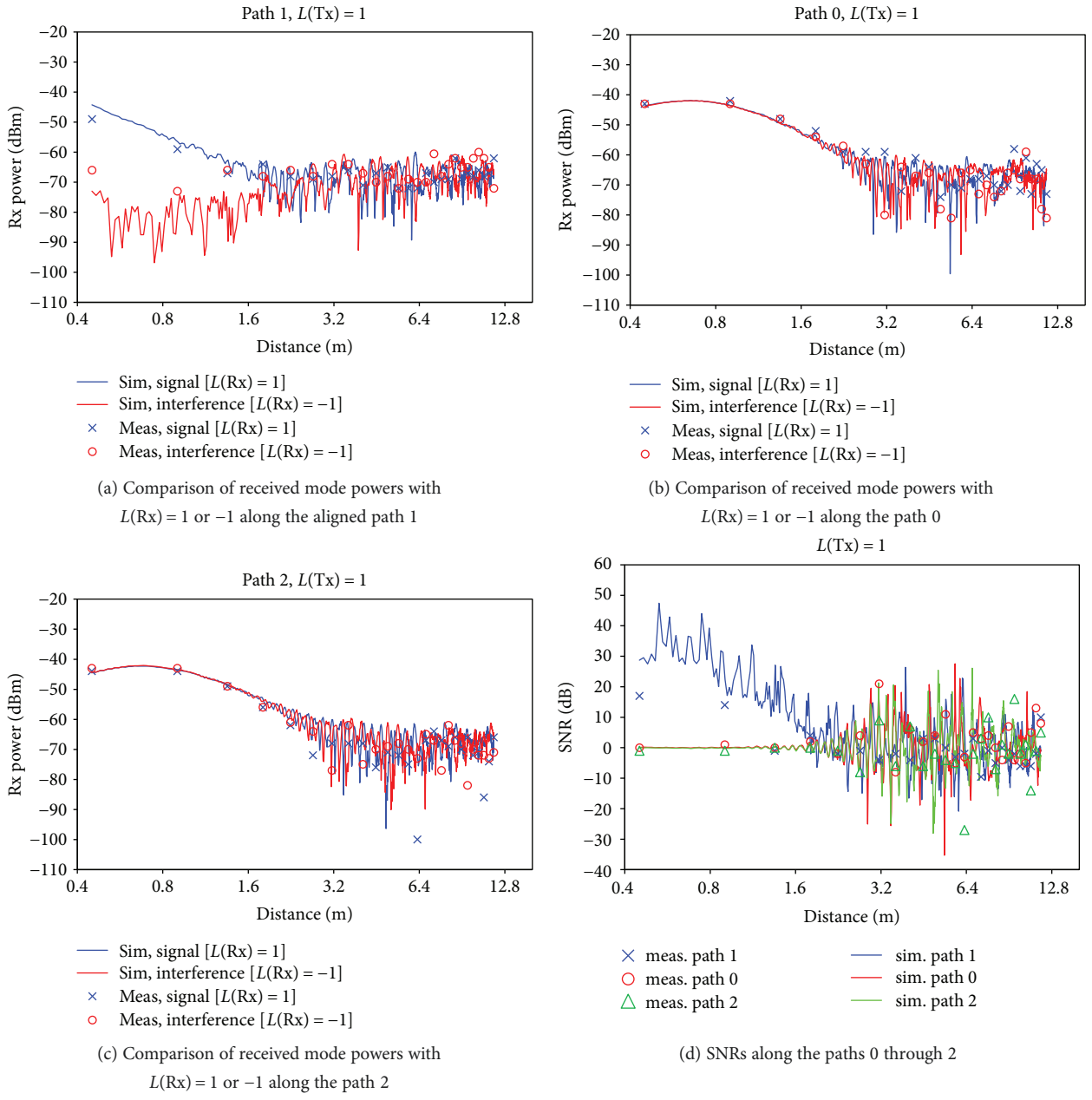

(a) Comparison of received mode powers with $L(\mathrm{Rx}) = 1$ or -1 along the aligned path 1

(b) Comparison of received mode powers with $L(\mathrm{Rx}) = 1$ or -1 along the path 0

(c) Comparison of received mode powers with $L(\mathrm{Rx}) = 1$ or -1 along the path 2

(d) SNRs along the paths 0 through 2

Figure 4: Received OAM mode powers along three paths in the lecture room for the transmitting mode of $L = 1$.

the height of 1.44 m above the floor. The transmitter generates OAM mode of $L = 1$ for this case. The two antennas face each other.

Figure 4 shows the received power levels along the three paths. The abscissa is the distance drawn on a logarithmic scale. The received powers are recorded every 45 cm with two OAM mode antennas of $L = 1$ and -1. For the path 1 where two antennas are aligned, the signal level for mode $L = 1$ is larger than that for $L = -1$ if the distance is smaller than 1.8 m. For larger distance, the power levels are comparable to each other. The measured data are compared with those of the ray-tracing simulator of Kim and Lee [13], which shows good agreement. Depending on the polarizations of the transmitted wave, the reflection coefficient of the wall or ground texture of the room becomes negative or positive. If the reflection coefficient becomes negative, the transmitted OAM mode with $L = 1$ changes the polarity. If the polarity of the OAM mode reversed, the OAM mode number also changes sign. For the path 0 and path 2, the received power levels of both OAM modes ($L = 1, -1$) become comparable from the beginning, which means that the transmit OAM mode ($L = 1$) is interpreted as a sum of $L = 1$ and $L = -1$ in the reference frame of the receiver. For these cases, orthogonality of the OAM modes at the transmitting antenna is broken on arriving at misaligned receiving antennas, which means increase of interference among receiving OAM mode antennas. The received power levels of path 1, however, are lower than those of the path 0 and the path 2, because the

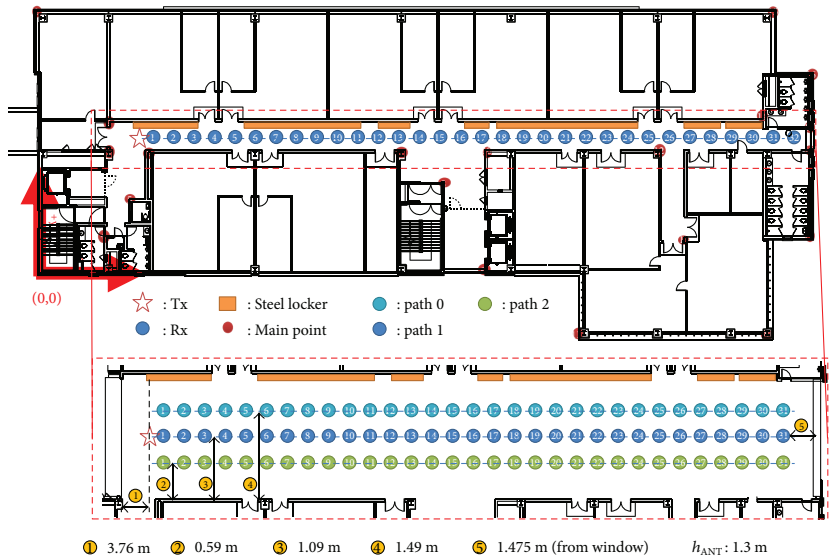

(a) Floor plan

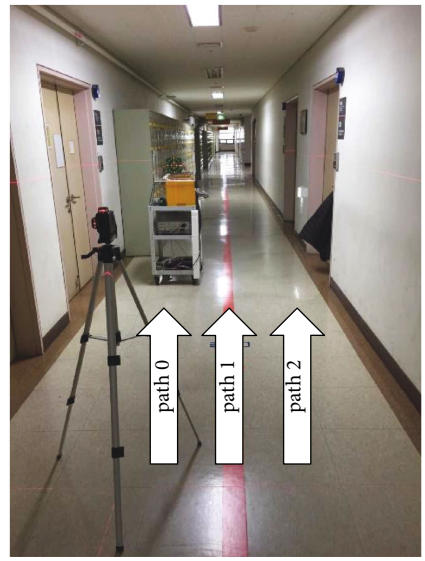

(b) Photo of the corridor

Figure 5: Measurement in the corridor.

radiation patterns of OAM modes ($L = 1$ and -1) have the highest level along off-axis directions [5].

For easy recognition of orthogonality among OAM modes, it is convenient to use the ratio of the received power of the same mode as that of the transmitter to the power sum of the other modes. The former corresponds to the desired signal power, and the latter becomes interference or noise. For convenience, the ratio is named as SNR (signal to noise ratio) and is given by the following.

$$\mathrm{SNR} \equiv \left(\frac{P_{l_{\mathrm{Rx}}=l_{\mathrm{Tx}}}}{\sum P_{l_{\mathrm{Rx}}\neq l_{\mathrm{Tx}}}} \right). \quad (1)$$

In Figure 4(d), SNR for the OAM mode $L = 1$ in the lecture room was shown. Away from the aligned path 1, SNRs decrease to 0 dB which means degradation of orthogonality. Even along the path 1, the orthogonality is broken over the distance of 1.35 due to the reflection on the wall, floor, and ceiling.

4. Propagation in the Corridor

The second measurement site is in the corridor as shown in Figure 5, which is 60 m long, with the ceiling height of 2.57 m and width of 2.51 m. The detailed floor plan is mentioned in [14]. The path 0 is 1.49 m apart from the right wall, the path 1 is 1.09 m, and the path 2 is 0.59 m apart. For this site, the same OAM modes $L = 1$ are transmitted.

As in the case of the lecture room, the path 1 is aligned with the transmitting antenna, but the other two paths (path 0 and 2) are misaligned. The power levels of the received OAM modes with $L = 1$ and -1 are recorded every 0.45 m. On the left wall, steel lockers are located. The

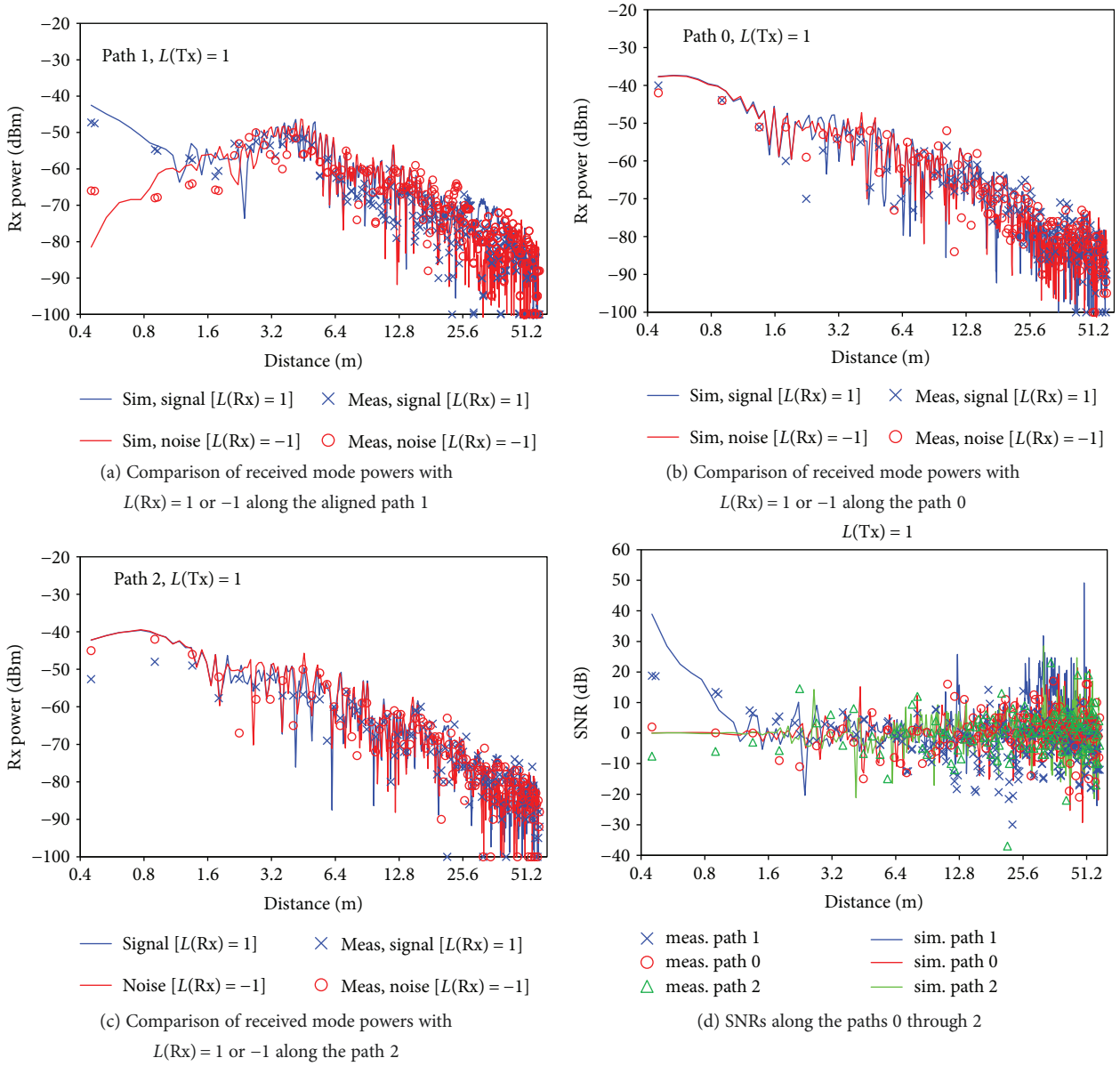

(a) Comparison of received mode powers with $L(\mathrm{Rx}) = 1$ or -1 along the aligned path 1

(b) Comparison of received mode powers with $L(\mathrm{Rx}) = 1$ or -1 along the path 0

(c) Comparison of received mode powers with $L(\mathrm{Rx}) = 1$ or -1 along the path 2

(d) SNRs along the paths 0 through 2

Figure 6: Received power levels of OAM modes for the transmitting mode of $L = 1$ in the corridor.

antennas are 1.29 m above the floor. Figure 6 shows the received OAM mode power levels with $L = 1$ and -1. For the aligned path 1, the received power of the OAM mode of $L = 1$ is higher than that of $L = -1$ within the distance of 1.2 m, which means the unbroken orthogonality property among received OAM modes. As the distance becomes larger, the power levels for both modes become comparable. For the displaced paths 0 and 2, the received power levels of the OAM modes $L = 1$ and $L = -1$ become comparable, which implies the broken orthogonality.

The measurements show that the orthogonality of OAM modes for receivers becomes broken along the misaligned paths for all cases. Even for the aligned path, the orthogonality becomes broken when the distance is larger than 1.2 m, which is due to the reflections from the wall, floor, and the ceiling. Compared with the case of the lecture room in Figure 4, the range of SNR larger than zero dB decreases from 1.8 m to 1.2 m. It is because the height and the width of the corridor are smaller than those of the lecture room. Due to the narrow corridor, more reflections occur before reaching the same distance.

5. Condition for Increased Coverage

It is found in the previous section that reflections should be suppressed to increase the range of orthogonality. To derive the condition, parametric studies are done using a ray-tracing simulator based on geometrical optics and uniform theory of diffraction [13]. We observe the range in which orthogonality among OAM modes is unbroken as the beam width of element antennas changes.

Figure 7 shows the SNR distribution for the lecture room in Figure 3. SNRs are obtained by moving the receiving antennas of OAM modes $L = 1$ and -1 with the transmitter

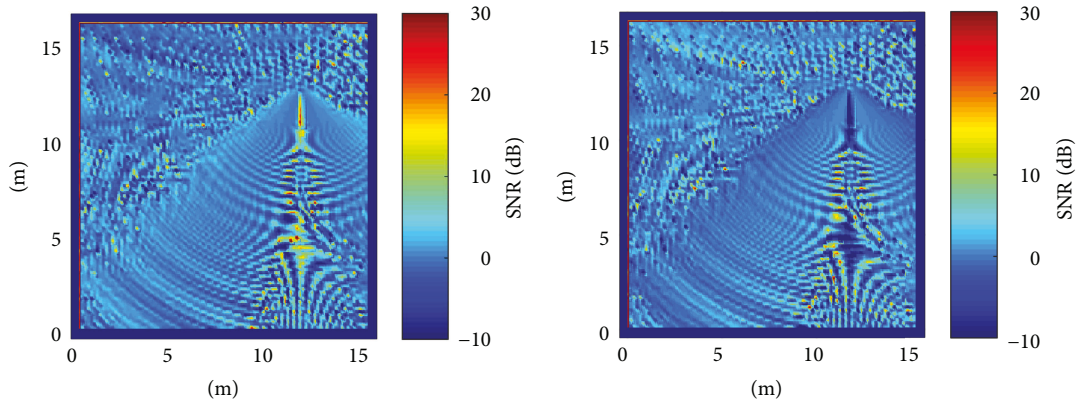

(a) SNRs for $L(\mathrm{Rx}) = 1$ (b) SNRs for $L(\mathrm{Rx}) = -1$

Figure 7: SNRs calculated for the lecture room with the transmitter of $L(\mathrm{Tx}) = 1$ using the antennas in Figure 1.

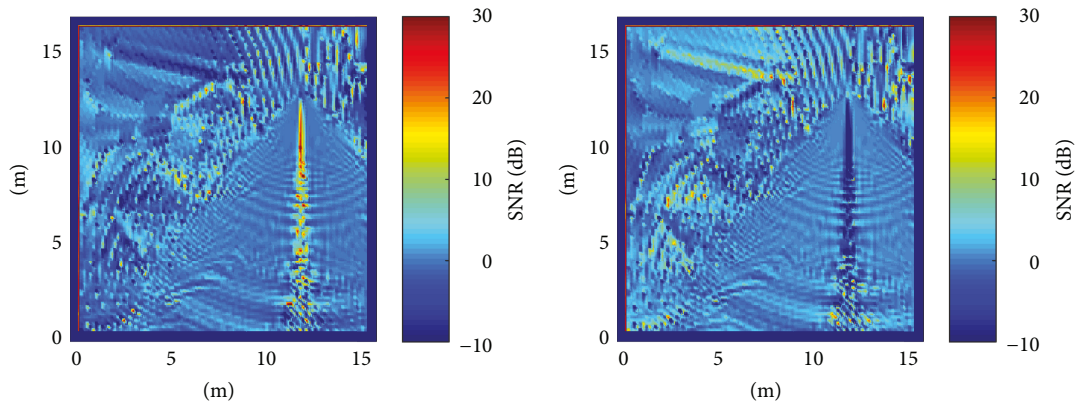

(a) SNRs for $L(\mathrm{Rx}) = 1$ (b) SNRs for $L(\mathrm{Rx}) = -1$

Figure 8: SNRs calculated for the lecture room with the transmitter of $L(\mathrm{Tx}) = 1$ using narrow beam width antennas (HPBW 10°).

of $L = 1$. To expedite the simulations, structures like the stairs and pillars are not modeled in the simulation. The color bar shows the range of SNR from −10 to 30 dB. Figure 7(a) shows the SNRs for receiver with $L = 1$. The SNR is observed high right in front of the transmitting antenna but has rapidly oscillating ripples for the distance larger than 1.8 m as shown in Figure 4(a). The ripples are due to reflections from the walls, ceiling, and floor. For the case of receiving antenna of $L = -1$, low SNR is observed right in front of the transmitting antenna but is then oscillating.

To consider the influence of antenna beam widths on the range of mode orthogonality, simulated SNRs for narrow beam width antennas (HPBW 10°) are given in Figure 8. The range of high SNR becomes larger. Due to the concentration of radiated field, reflections decrease in Figure 8(a). The SNR for $L = -1$ is kept low along the main beam direction, but is oscillating after reflections.

The high SNR in the narrow region can increase capacity of radio transmission system by using arrays of OAM antennas as in [15–17].

As to the case of the OAM mode $L = 2$, simulated results are given in Figure 9. Due to the divergent radiation pattern of $L = 2$ [4], the range of high SNR decreases much from that of $L = 1$.

Figure 10 shows SNRs for the corridor in Figure 5 obtained from OAM modes of $L = -1$ and 1 with the element antenna beam width changed. Beam widths of element antennas are specified by field of view (FOV) angles of the radiation pattern. Three cases considered are FOV angles of 10°, 5°, and 3°. As the FOV angles decrease, the ranges of SNR that exceeds 10 dB become larger from 2.9 m to 9.6 m. Larger SNR means better orthogonality among received OAM modes. The simulations imply that to increase the coverage of OAM mode antennas without breaking the orthogonality, the beam widths of the antennas should be small.

6. Conclusion

In this paper, we present the measurement and simulation results of indoor propagation of OAM mode waves. To extract the merit of increased capacity of OAM mode antennas, alignment of antennas and suppression of reflection should be satisfied. If any of those two conditions are not fully satisfied, the coverage where OAM mode

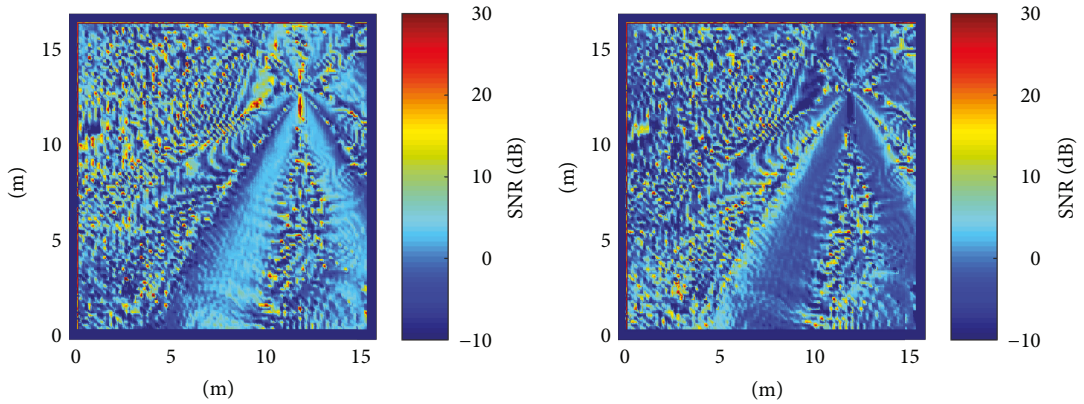

(a) SNRs for $L(\mathrm{Rx}) = 2$

(b) SNRs for $L(\mathrm{Rx}) = 1$

Figure 9: SNRs calculated for the lecture room with the transmitter of $L(\mathrm{Tx}) = 2$.

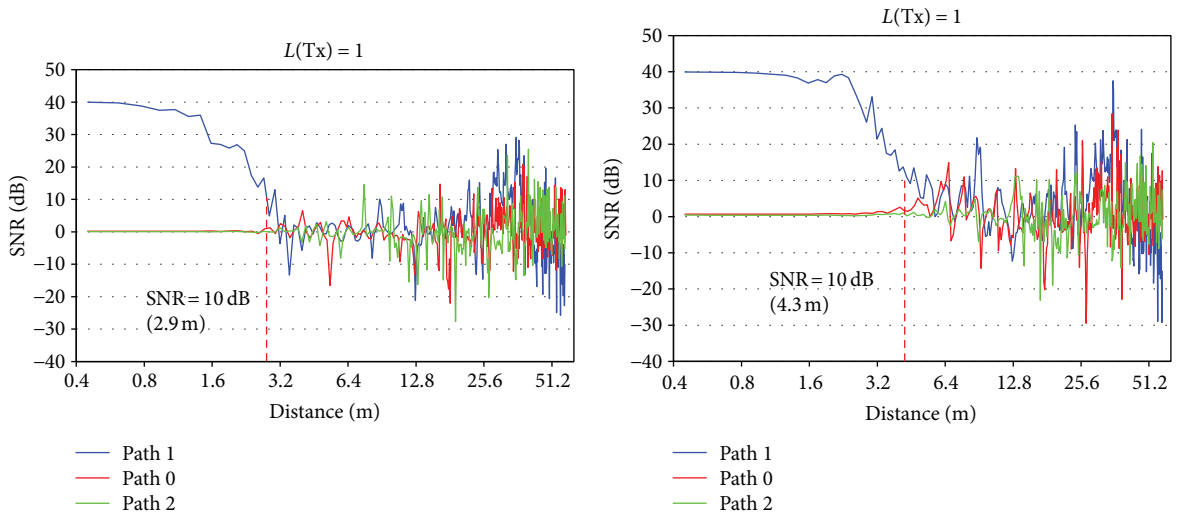

(a) SNR for FOV angle of 10°

(b) SNR for FOV angle of 5°

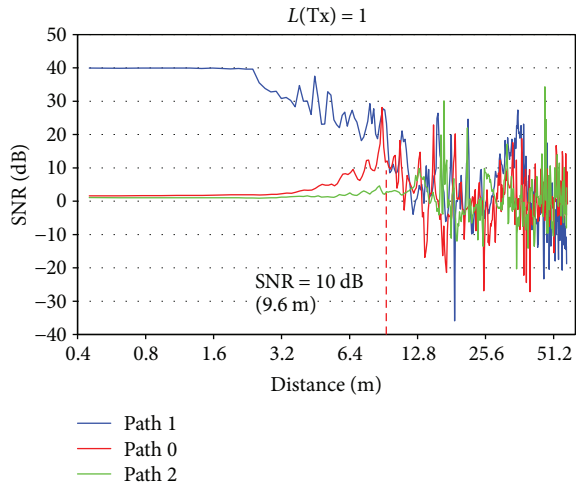

(c) SNR for FOV angle of 3°

Figure 10: SNRs calculated for the corridor when the element antennas of OAM modes have FOV angles of 10°, 5°, and 3°. The OAM mode number of the transmitting antenna (L_{Tx}) is zero.

orthogonality is conserved decreases. It is found that the coverage increases with narrow beam antennas even in the multipath environment.

Conflicts of Interest

The authors declare that there is no conflict of interests regarding the publication of this article.

Acknowledgments

This work was supported by the Sogang University Research Grant of 2017 (201710129.02).

References

[1] M. W. Beijersbergen, R. P. C. Coerwinkel, M. Kristensen, and J. P. Woerdman, "Helical-wave front laser beams produced with a spiral phase plate," *Optics Communications*, vol. 112, no. 5-6, pp. 321–327, 1994.

[2] L. Allen, M. W. Beijersbergen, R. J. C. Spreeuw, and J. P. Woerdman, "Orbital angular momentum of light and the transformation of Laguerre-Gaussian laser modes," *Physical Review A*, vol. 45, no. 11, pp. 8185–8189, 1992.

[3] G. A. Turnbull, D. A. Robertson, G. M. Smith, L. Allen, and M. J. Padgett, "The generation of free-space Laguerre-Gaussian modes at millimeter-wave frequencies by use of a spiral phase plate," *Optics Communications*, vol. 127, no. 4–6, pp. 183–188, 1996.

[4] B. Thidé, H. Then, J. Sjöholm et al., "Utilization of photon orbital angular momentum in the low-frequency radio domain," *Physical Review Letters*, vol. 99, no. 8, article 087701, 2007.

[5] S. M. Mohammadi, L. K. S. Daldorff, J. E. S. Bergman et al., "Orbital angular momentum in radio—a system study," *IEEE Transactions on Antennas and Propagation*, vol. 58, no. 2, pp. 565–572, 2010.

[6] Q. Bai, A. Tennant, and B. Allen, "Experimental circular phased array for generating OAM radio beams," *Electronics Letters*, vol. 50, no. 20, pp. 1414-1415, 2014.

[7] W. Wei, C. Brousseau, K. Mahdjoubi, and O. Emile, "Generation of OAM waves with circular phase shifter and array of patch antennas," *Electronics Letters*, vol. 51, no. 6, pp. 442-443, 2015.

[8] J. Wang, J.-Y. Yang, I. Fazal et al., "Experimental demonstration of 100-Gbit/s DQPSK data exchange between orbital-angular-momentum modes," in *Optical Fiber Communication Conference Optical Society of America*, Los Angeles, CA, USA, March 2012.

[9] J. Wang, J. Y. Yang, I. M. Fazal et al., "Terabit free-space data transmission employing orbital angular momentum multiplexing," *Nature Photonics*, vol. 6, no. 7, pp. 488–496, 2012.

[10] F. E. Mahmouli and S. D. Walker, "4-Gbps uncompressed video transmission over a 60-GHz orbital angular momentum wireless channel," *IEEE Wireless Communications Letters*, vol. 2, no. 2, pp. 223–226, 2013.

[11] Y. Yan, G. Xie, M. P. J. Lavery et al., "High-capacity millimeter-wave communications with orbital angular momentum multiplexing," *Nature Communications*, vol. 5, p. 4876, 2014.

[12] Y. Yan, L. Li, G. Xie et al., "Experimental measurements of multipath-induced intra- and inter-channel crosstalk effects in a millimeter-wave communications link using orbital-angular-momentum multiplexing," in *2015 IEEE International Conference on Communications (ICC)*, pp. 1370–1375, London, UK, June 2015.

[13] H. Kim and H. S. Lee, "Accelerated three dimensional ray tracing techniques using ray frustums for wireless propagation models," *Progress in Electromagnetics Research*, vol. 96, pp. 21–36, 2009.

[14] S.-h. Min, H. Kim, H. Lee et al., "Spatial and temporal characterization of indoor millimeter wave propagation at 24 GHz," *International Journal of Antennas and Propagation*, vol. 2016, Article ID 2318731, 10 pages, 2016.

[15] Z. Zhang, S. Zheng, Y. Chen, X. Jin, H. Chi, and X. Zhang, "The capacity gain of orbital angular momentum based multiple-input-multiple-output system," *Scientific Reports*, vol. 6, article 25418, p. 1, 2016.

[16] Y. Ren, L. Li, G. Xie et al., "Line-of-sight millimeter-wave communications using orbital angular momentum multiplexing combined with conventional spatial multiplexing," *IEEE Transactions on Wireless Communications*, vol. 16, no. 5, pp. 3151–3161, 2017.

[17] X. Ge, R. Zi, X. Xiong, Q. Li, and L. Wang, "Millimeter wave communications with OAM-SM scheme for future mobile networks," *IEEE Journal on Selected Areas in Communications*, vol. 35, no. 9, pp. 2163–2177, 2017.